UNDULATORS FOR THE BESSY SOFT-X-RAY FEL

J. Bahrdt#, W. Frentrup, A. Gaupp, B. Kuske, A. Meseck, M. Scheer, BESSY, Berlin, Germany

Abstract

BESSY plans to build a linac based Soft-X-ray FEL facility. Three FEL lines will cover the energy range between 24eV and 1000 eV. The FELs are operated in a high gain harmonic generation scheme providing short pulses and stable operation. This paper describes the undulator systems for the FELs.

INTRODUCTION

The time structure of a high gain harmonic generation FEL is determined by the time structure of the Laser system. The FWHM of the FEL radiation is expected to be below 30 fs. Furthermore, the shot to shot intensity variations are small compared to a SASE FEL scheme. The three FELs will be operated at electron energies of 1GeV (LE-FEL) and 2.3GeV (ME-FEL and HE-FEL), respectively. They consist of 2, 3, and 4 stages with a modulator, a dispersive section and a radiator each followed by a final amplifier (table 1).

The photon energy tuning will be done via gap motion. For the HE-FEL the electron beam energy has to be modified additionally to provide the full tuning range. The last radiators and the final amplifiers will be devices with full polarization control. The other modules which are responsible for the electron beam bunching are planar undulators.

Table 1: Parameters of the BESSY Soft-X-Ray FEL. Period lengths (1st number) and section lengths (2nd number) are given in mm and m, respectively [1].

Device	LE-FEL		ME-FEL		HE-FEL	
Energy range	24-120 eV		100-600 eV		500-1000 eV	
	Modulator	Radiator	Modulator	Radiator	Modulator	Radiator
Stage 1	80 / 1.60	62 / 3.47	122 / 2.56	92 / 3.86	122 / 2.20	92 / 3.86
Stage 2	62 / 1.61	50 / 3.45	92 / 2.21	70 / 2x3.78	92 / 2.01	70 / 3x3.80
Stage 3			70 / 2.31	50 2x3.75	70 / 2.1	50 / 3x 3.1
Stage 4					50 / 2x2.65	28.5 / 2x 3.28
Final amplifier	50 / 3x3.85		50 / 3x3.85		28.5 / 5x3.65	
Total length / m	21.68		37.55		60.98	

LAYOUT OF THE UNDULATORS

Since all gaps are variable a separated function focussing scheme has been adopted. The quadrupoles of the FODO structure are located between the undulator segments. Permanent magnet phase shifters with adjustable magnetic gaps provide the correct phase adaption between the undulator segments. Correction coils, and diagnostic systems are located in the intersections as well.

A dogleg collimator with a spatial and an energy collimation stage protects the magnets from being hit by dark current electrons.

MAGNETIC DESIGN

The modulators and the first radiators will be pure permanent magnet structures. The last radiator and the final amplifier are of the APPLE III type (see figure 1) [2]. An APPLE III provides the same flexibility concerning the polarization control as an APPLE II but the maximum field is larger at the expense of a reduced access from the side. In a linac driven FEL a circular beam pipe can be used and more magnetic material can be located close to the electron beam. Side access to the magnetic structure is needed only for Hall probe measurements and for the chamber support. A minimum magnetic gap at the side of only 5.4mm can be realized still providing the space for a 10.4mm diameter tube. The magnetic field can be further enhanced by tilting the magnetization direction to 45 degrees. The reverse fields in an APPLE III structure require a more stable material compared to an APPLE II undulator and as a consequence the remanence of the material is about 6% lower. Nevertheless, the effective magnetic field is a factor of 1.4 higher than for an APPLE II with a gap of 10.4mm.

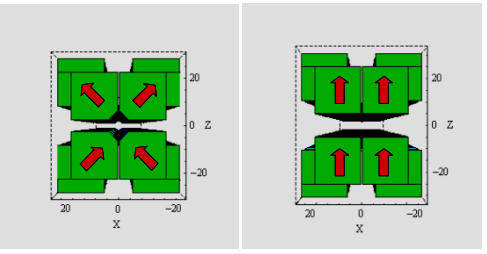

Figure 1: Magnetic structure of an APPLE III (left) compared to an APPLE II design (right).

#bahrdt@bessy.de

The magnetic field of an APPLE III undulator can be parametrized with:

$$B(T) = a \cdot \exp(b \cdot (gap/\lambda_0) + c \cdot (gap/\lambda_0)^2)$$

useing the parameters of table 2.

The parameters of table 2 have been evaluated with the 3D-code RADIA [3] for remanence = 1.13T and 1.19T (longitudinally and 45° magnetized blocks), block dimensions = 40x40mm^2, minimum vertical distance = 5.4mm, free aperture = 10.4mm. The parameters are valid for period lengths of 20mm $\leq \lambda_0 \leq$ 50mm.

Table 2: Field parameters of the APPLE III design

	hor. lin.	vert. lin.	circular	lin. 45°
A	2.481	2.035	2.209	1.569
B	-6.258	-6.576	-6.400	-6.392
C	0.112	0.602	0.285	0.231

The horizontal roll off of the vertical field component is larger for an APPLE III than for an APPLE II whereas the roll off of the horizontal field component is smaller (figure 2). For the HE-FEL a relative alignment accuracy of the undulator modules of ±20µm is required. The undulator segments will be mounted onto remote controlled transversely movable stages in order to meet this tight tolerance. The indication for a correct alignment will be the FEL output.

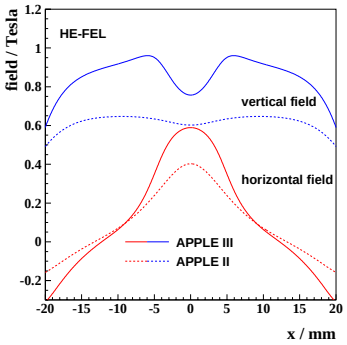

Figure 2: Comparison of the transverse field profiles of the APPLE II and the APPLE III design evaluated for the HE-FEL.

SOURCE CHARACTERIZATION

Three dimensional FEL codes provide information about the electric field distribution at the end of the final amplifier, $z=z_0$. This point is not the location of the photon beam waist. The beamline designer needs to know the exact location and the size of the photon beam waist in order to maximize the brightness at the sample. This information can be derived from the results of a longitudinal propagation of the electric field distribution. There are two ways to proceed:

1: Integration of the diffraction equation of Fresnel and Kirchhoff:.

$$\vec{E}(x',y') = \frac{1}{\lambda}\int_{-\infty}^{\infty}\int_{-\infty}^{\infty}\vec{E}(x,y)\frac{e^{i\vec{k}(\vec{r}-\vec{r}')}}{|\vec{r}-\vec{r}'|}\cos(\beta)\cdot dx\cdot dy$$

2: Application of Fourier optic methods.

A FFT yields the angle distribution of the FEL output

$$\vec{E}_0(\nu_x,\nu_y) = \int_{-\infty}^{\infty}\int_{-\infty}^{\infty}\vec{E}(x,y)\cdot e^{-2\pi i(\nu_x x+\nu_y y)}dx\cdot dy$$

This distribution is multiplied by a factor which represents a longitudinal drift of Δz.

$$\vec{E}(\nu_x,\nu_y) = \vec{E}_0(\nu_x,\nu_y)\cdot e^{2\pi i\cdot\Delta z\cdot\sqrt{1/\lambda^2-\nu_x^2-\nu_y^2}}$$

An inverse FFT provides the spatial distribution at $z=z_0+\Delta z$.

$$\vec{E}(x',y') = \int_{-\infty}^{\infty}\int_{-\infty}^{\infty}\vec{E}(\nu_x,\nu_y)\cdot e^{2\pi i\cdot(\nu_x x+\nu_y y)}\cdot d\nu_x\cdot d\nu_y$$

The second method is much faster in cases where the transverse dimension of the photon beam size does not change too much within Δz. The following results are derived with this method.

To study the development of the radiation properties within the final amplifier time dependent GENESIS simulations [4] have been performed for various lengths L of the LE-FEL final amplifier of $L=L_0$-$81\lambda_0$, L_0-$60\lambda_0$, L_0-$40\lambda_0$, L_0-$20\lambda_0$ and L_0, where L_0 is the length of the final amplifier given in table 1.The power distributions are plotted in figure 3. The corresponding electric fields have been propagated by amounts of Δz with -30m ≤ Δz ≤ +20m and the intensities have been projected onto the horizontal and the vertical plane. The first and second moments of these projections have been evaluated and the results for slice 4 are plotted in figure 4. Similar numbers have been obtained for slices 2,3 and 5.

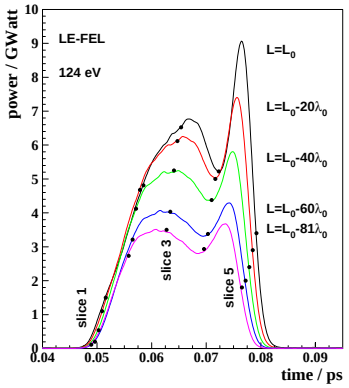

Figure 3: GENESIS simulations for different lengths L of the final amplifier. The electric fields of five slices (black circles) have been propagated.

The photon beam waist is located several meters upstream from the FEL end and this distance increases with L. As a consequence the brightness at the sample can be increased by a factor of two if the waist is focussed instead of the FEL end.

The photon beam size increases with the length of the final amplifier (figure 4). This might be partly due to the increasing electron beam size which varies between 115 and 127μm horizontally and between 105 to 130μm vertically for $L_0\text{-}81\lambda_0 \le L \le L_0$.

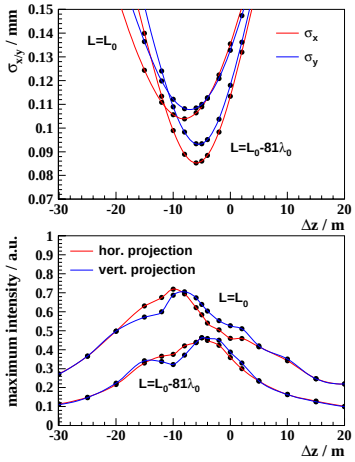

Figure 4: Photon beam size (top) and maxima of the projected intensity (bottom) versus longitudinal distance to the final amplifier end. The data of slice 4 are plotted.

The photon beam divergence decreases with L and the phase space product σσ' is nearly independent of L for slice 4 (figure 5) and also for slices 2, 3 and 5. For a diffraction limited beam we expect a product of $\sigma\sigma' = \lambda/4\pi$ = 0.8nm (124eV). Based on the GENESIS simulations we obtain for each of the slices 2, 3, 4 and 5 a product of about 1.25nm which is close to the theoretical limit.

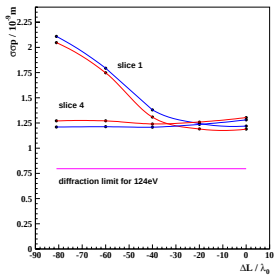

Figure 5: Phase space volume of the LE_FEL radiation for various lengths of the final amplifier.

For $L = L_0\text{-}81\lambda_0$ slice 1 is far below saturation. The waist is located close to the FEL end and moves further upstream for increasing L (figure 6). The phase space product of slice 1 is a factor of 2.5 above the diffraction limit for $L = L_0\text{-}81\lambda_0$ and approaches the value of the slices 2-5 for increasing L (figure 5).

The specific case of the LE-FEL at 124eV indicates that the location of the waist moves upstream relative to the FEL end when the FEL goes into saturation. A distance of 10m between the FEL end and the waist is significant and has to be regarded in a monochromator design. The question has to be answered whether the location of the waist moves with photon energy which would imply the necessity of a variably focussing beamline optic. Further studies for more photon energies and also for the ME-FEL and the HE-FEL are in progress.

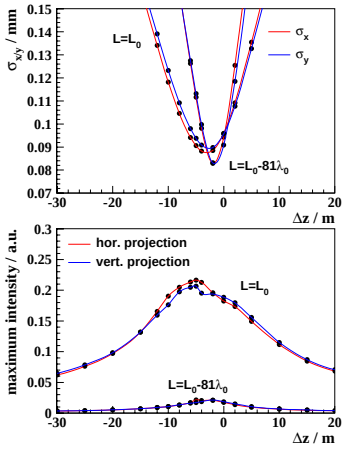

Figure 6: Photon beam size (top) and maxima of the projected intensity (bottom) versus longitudinal distance to the final amplifier end. The data of slice 1 are plotted.

FIELD OPTIMIZATION

The field tuning for the planar modulators and the radiators of the first stages is straight forward [5]. Shimming of the last radiator and the final amplifier is more complicated due to several reasons: i) Iron shims can not be used as usual because the signature changes with magnet row shift. ii) the shims do not stick by magnetic forces. iii) The shims can not be applied directly above or below the electron beam because the magnet rows are separated by a slit of 1mm. iv) The field integrals depend on the shift of the magnet rows which is due to the non unity of the magnetic permeability.

Magnet sorting techniques based on detailed field data of individual magnets are essential for these devices to reduce the work on shimming after assembly. At BESSY a precise set-up for the characterization of magnet block inhomogeneities has been developed [6]. Using the inhomogeneity data together with the Helmholtz coil data in a simulated annealing code the best magnet configuration is evaluated. It has been demonstrated at BESSY that even for devices consisting of more than 1000 individual blocks the field integrals can be predicted with an accuracy of ± 1.5Gm [6]. The prediction is based only on single block data and no further field measurement and resorting has been performed during magnet assembly. The remaining field errors can be removed in three steps:

1: Trajectory and phase errors are minimized with transverse block movements (virtual shimming).

2: The endpoles can be designed such that the field integral variation with gap is small [1] [7]. The remaining

shift dependent terms are minimized with iron shims which are glued onto the magnets.

3: Shift independent field integrals are removed with permanent magnet arrays at both ends of the device.

These techniques have been applied to several APPLE II undulators at BESSY and they are documented in detail in [6].

SUPPORT AND DRIVE SYSTEM

The support structure (cast iron) consists of a base frame carrying two C-frames. The magnetic structures will have a length of up to 4m. The magnet girders will be made from aluminum. The deflection is minimized with four supports (instead of two) using two cross bars. This design has already been implemented successfully at BESSY.

Four longitudinal drive systems give the flexibility to move each row individually. This provides full polarization control for the user. Parallel motion of two rows changes the polarization from horizontal linear to circular and to vertical linear. Anti-parallel motion tilts the linear polarization vector continuously from 0° to 90°. Sometimes, the orientation of the sample is not well known. In these cases it is useful to rotate the polarization vector by more than 90°. With 4 motors a rotation of 180° is possible.

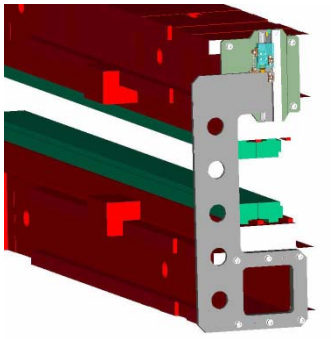

Figure 7: The new gap measurement system as implemented at the BESSY UE49 undulator.

Two servo motors provide the gap tunability. The gaps of the individual undulator sections have to be adjusted with a relative accuracy better than 3µm. This tight tolerance can not be achieved with measurement systems used so far. Rotary encoders suffer from backlash of gearboxes and linear encoders coupled to the upper and the lower I-beam do not follow Abbe's comparator principle. We have developed a new measurement system where the linear encoder is located directly above the electron beam thus following Abbe's comparator principle. The system recently installed at the BESSY APPLE II undulator UE49 (figure 7) demonstrated a gap reproducibility of ±1µm independent of the gap history (figure 8).

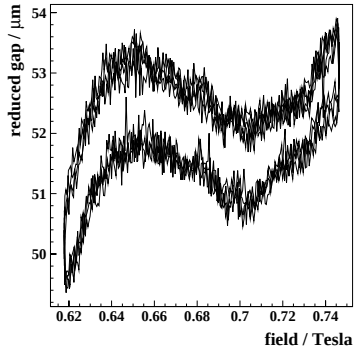

Figure 8: Measured gaps versus magnetic field for several cycles of gap opening and closing. A 4th order polynomial has been subtracted from the raw data to show the residual error.

REFERENCES

[1] The BESSY Soft-X-Ray Free Electron Laser, Technical Design Report, Berlin, Germany, March, 2004.

[2] J. Bahrdt, W. Frentrup, A. Gaupp, B. Kuske, A. Meseck, M. Scheer, "Undulators for the BESSY SASE-FEL Project", 8th International Conference on Synchrotron Radiation Instrumentation, San Francisco, Cal., 2003, AIP 0-7354-0180-2/04, p215.

[3] P. Elleaume, O. Chubar, J. Chavanne, "Computing 3D magnetic fields from insertion devices", Proc. of the 1997 PAC, Vancouver, Canada (1997) 3509-3511. O. Chubar, P. Elleaume, J. Chavanne, "A three-dimensional magnetostatics computer code for insertion devices", J. Synchr. Rad. 5 (1998) 481-484.

[4] A. Meseck, B. Kuske, these proceedings

[5] D.C. Quimby, S.C. Gottschalk, F.E. James, K.E. Robinson, J.M. Slater, A.S. Valla, "Development of a 10-meter wedged-pole undulator", Nucl. Instr. and Meth., A285 (1989) 281-289. S.C. Gottschalk, D.C. Quimby, K.E. Robinson, J.M. Slater, "Wiggler error reduction through shim tuning", Nucl. Instr. and Meth., A296 (1990) 579-587. B. Diviacco, R.P. Walker, "Recent advances in undulator performance optimization", Nucl. Instr. and Meth., A368 (1996) 522-532. J. Chavanne, P. Elleaume, "Undulator and wiggler shimming", Synchr. Rad. News, Vol.8 No.1 (1995) 18-22.

[6] J. Bahrdt, W. Frentrup, A. Gaupp, M. Scheer, "Magnetic field optimization of permanent magnet undulators for arbitrary polarization", Nucl. Instr. and Meth. A, 516 (2004) 575-585.

[7] J. Chavanne, P. Elleaume, P. Van Vaerenbergh, "End field structures for linear/helical insertion devices", Proc. of the PAC, New York, NY, USA (1999) 2665-2667.